Scientific Research Publishing

Smart Grid and Renewable Energy, 2026, 17(3), 29-41
https://www.scirp.org/journal/sgre
ISSN Online: 2151-4844
ISSN Print: 2151-481X

Impact of Irradiance-Temperature Coupling and Magnetic Field Study in PV Generators

Mamadou Osias Sory[1], Alain Diasso[2], Soulemani Sangare[1], Moussa Ouedraogo[1], Raguilignaba Sam[1,2], François Zougmore[1]

[1]Department of Physics, Laboratory of Heliophysical Materials and Environment, Nazi BONI University, Bobo-Dioulasso, Burkina Faso
[2]Department of Physics, Laboratory of Materials and Environment, Joseph KI-ZERBO University, Ouagadougou, Burkina Faso
Email: sory.mamadou.etu@univ-bobo.gov.bf

How to cite this paper: Sory, M.O., Diasso, A., Sangare, S., Ouedraogo, M., Sam, R. and Zougmore, F. (2026) Impact of Irradiance-Temperature Coupling and Magnetic Field Study in PV Generators. *Smart Grid and Renewable Energy*, **17**, 29-41.
https://doi.org/10.4236/sgre.2026.173003

Received: January 22, 2026
Accepted: March 10, 2026
Published: March 13, 2026

Abstract

This work presents a theoretical study of the combined impact of the magnetic field and the correlation between solar irradiance and temperature on the excess minority electron density within the base of a polycrystalline silicon solar cell with parallel junction. The results reveal a gradual decrease in electron density with increasing magnetic field intensity, for various irradiance values, whether coupled with temperature or not. Electron density vanishes at 1.2 mT under constant temperature conditions, and beyond 1.2 mT when temperature varies jointly with irradiance. The electron density is consistently higher under constant temperature than when temperature is coupled with irradiance, a phenomenon attributed to the rise in thermal recombination. While the reduction in carrier density is also explained by the Lorentz force, which facilitates electron confinement and hinders their collection, light intensity conversely stimulates carrier generation, thereby increasing photocurrent density and photovoltage. The irradiance-temperature coupling may induce significant energy losses and should be considered in the design and optimization of photovoltaic cells. Although purely theoretical and pending experimental validation, this study provides valuable insights for refining technical and economic assessments in the development of preliminary solar projects.

Keywords

Photovoltaic Generators, Coupling, Irradiance, Temperature

1. Introduction

Exposed to extreme environmental conditions such as elevated temperatures, intense irradiance, and electromagnetic fields, solar cells experience a direct degra-

dation in performance due to these exogenous factors [1] [2]. Martial *et al*. [1] highlighted the combined influence of the magnetic field and the electric field gradient induced by intense photogeneration on the electrical parameters of a silicon solar cell under high light concentration. This study led to the formulation of new analytical expressions related to the continuity equation, photocurrent, and photovoltage. In a similar vein, Sawadogo *et al*. [3]-[5] demonstrated that, under extreme light concentration, the combined effects of the induced electric field and temperature result in a significant degradation of photovoltaic performance, following a complex thermal dynamic linked to the shift in operating point and intrinsic parameter variation. Soro *et al*. [6], for his part, established that the simultaneous increase in base temperature and magnetic field intensity in a concentrated solar cell leads to a deterioration in electrical performance, despite a localized increase in photocurrent under certain conditions.

In parallel, Zouma *et al*. [7] showed that the combination of extreme light concentration and a constant magnetic field profoundly alters the distribution of minority carriers and the electrical performance of bifacial silicon solar cells, resulting in new analytical expressions for rear-side illumination. Subsequent work by Zoungrana *et al*. [8] [9] revealed nonlinear variations in photovoltaic performance, notably that rising temperature reduces carrier mobility [5], while irradiance alters photogeneration profiles and the magnetic field affects diffusion and recombination phenomena [7].

In response to these constraints, bifacial cells and tandem structures emerge as promising solutions to mitigate the aforementioned deleterious effects. In this regard, research by Zouma *et al*. [7] demonstrated that rear-side illumination, combined with three-dimensional modeling, enables optimized management of thermal gradients and carrier fluxes. Furthermore, dual-absorber cells (CZTSSe/CIGS) incorporating a BSF layer [10] achieve efficiencies exceeding 35%, thanks to meticulous optimization of layer thicknesses and concentrations. Finally, Silvaco-assisted modeling of a CIGS solar cell shows that by replacing the CdS layer, adding anti-reflective coatings, and implementing a trapezoidal gallium gradient profile [11], device efficiency can reach 19.21%, with a 36.24% improvement attributed to base structuring. Furthermore, Diasso *et al*. [12] examined the combined influence of external magnetic field and air mass on carrier density, transient voltage, and electrical parameters in a polycrystalline solar cell, based on a three-dimensional model solved using Green's functions under multispectral flash illumination, with the aim of optimizing charge collection and overall performance in high-altitude environments. More recently, Ouedraogo *et al*. [13], through a theoretical study, investigated the joint impact of magnetic field and temperature on carrier density in a radial polycrystalline silicon.

Current studies on the effects of temperature, irradiance, and magnetic field on photovoltaic cells are primarily based on theoretical models that fail to account for the correlation among these parameters. In a climate context marked by extreme fluctuations, such coupling becomes critical, as it may limit the relevance of

conventional approaches. The present study offers an in-depth analysis of the combined effect of the magnetic field and the correlation between solar irradiance and temperature on the excess minority electron density within the base of a polycrystalline silicon solar cell with parallel junction. The adopted approach relies on a three-dimensional analytical model in a static regime, based on several simplifying assumptions, notably a quasi-neutral base and the exclusion of emitter contribution in generation and recombination phenomena. This modeling enables the derivation of rigorous expressions for carrier density, and by extension, for photocurrent and photovoltage. The primary objective of this study is to provide a precise evaluation of the impact of the coupling between irradiance G, temperature T, and magnetic field B on the performance of a photovoltaic cell, with the aim of enriching existing models and opening new avenues for optimization under extreme climatic conditions.

2. Model and Assumptions

2.1. Analytical Formulation

As part of this three-dimensional modeling, the study focuses on a bifacial solar cell composed of polycrystalline silicon, consisting of an assembly of grains with varied morphologies and dimensions, yet exhibiting homogeneous electrical properties [14]. These grains, characterized by square cross-sections and a given thickness H, are separated by intergranular boundaries [9], which constitute preferential sites for recombination phenomena. This structural configuration justifies the adoption of a Cartesian coordinate system for the analytical treatment. **Figure 1** illustrates a representative segment of a grain, where the recombination planes are defined as the adjacent surfaces between two perpendicular grains, located at positions $x = \pm\frac{a}{2}$ and $y = \pm\frac{a}{2}$. Interface recombination is modeled using a uniform surface recombination velocity ($S_{gx} = S_{gy} = S_g$) [7], assumed to be independent of solar irradiance. This assumption allows the imposition of linear boundary conditions in the continuity equations. The diffusion of minority carriers is thus governed by temperature and the intensity of the magnetic field. For the sake of simplification, the contributions of the emitter and the space-charge region are neglected, with the analysis focusing exclusively on the base of the cell. It is subjected to uniform, non-concentrated front-side illumination and to a variable external magnetic field oriented perpendicularly to the depth of light penetration [9] [15]. Light enters the junction at the plane ($z = 0$).

In the present model, the magnetic field is applied perpendicularly to the (xOz) plane, that is, parallel to the junction, so that the base doping level is considered uniform. This leads to a quasi-zero crystalline electric field.

Temperature is correlated with solar irradiance through the following relation [16]-[18]:

$$T = T_a + \frac{\text{NOCT} - 20}{800} \times G = T_a + \frac{\text{NOCT} - 20}{800} \times 1000C \tag{1}$$

where NOCT is the cell's nominal operating temperature, specified by the manufacturer. It is determined under standardized test conditions of 800 W/m^2 irradiance, and a wind speed of 1 m/s, T is the real-time temperature of the solar cell in Kelvin (K), T_a is the ambient temperature in Kelvin (K), G is the solar irradiance in W.m^{-2} or in suns with $1C = 1000\ \mathrm{W}\cdot\mathrm{m}^{-2}$.

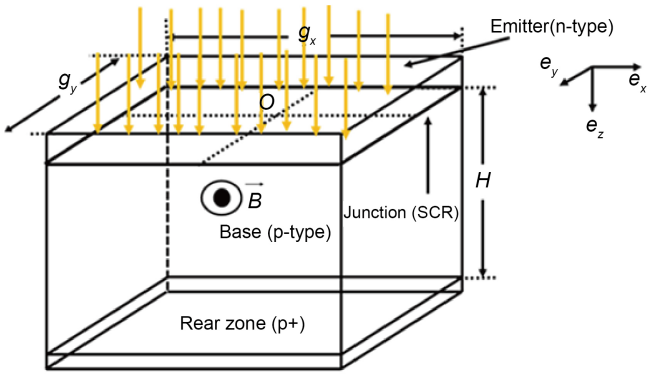

Figure 1. Theoretical model of a grain segment in a polycrystalline silicon photovoltaic cell.

2.2. Determination of Carrier Density

2.2.1. Continuity Equation

Under conditions of light intensity and external magnetic field, the excess minority carrier density $\delta(x,y,z)$ generated within the base is governed by the following continuity equation:

$$\frac{\partial^2\delta_n(x,y,z)}{\partial x^2}+\theta\frac{\partial^2\delta_n(x,y,z)}{\partial y^2}+\frac{\partial^2\delta_n(x,y,z)}{\partial z^2}-\frac{\delta_n(x,y,z)}{L^2(T,B)}=\frac{g(z)}{D(T,B)} \tag{2}$$

where

$$\theta(T,B)=1+\left(\mu(T)B\right)^2;\quad D(T,B)=\frac{D(T)}{\theta(T,B)}\quad L(T,B)=\frac{L(T)}{\theta(T,B)}\quad \text{and}$$

$$g_n(z)=G\times\sum_{i=1}^{3}a_i\mathrm{e}^{-b_iz} \tag{3}$$

with

$$\mu(T)=\mu_0\left(\frac{T}{T_0}\right)^{-m} \tag{4}$$

$g(z)$ denotes the generation rate [19] of minority carriers; G represents the number of suns or the solar irradiance [3] [4] [20] [21], suns; a_i and b_i are constants [18] [22] tabulated in the spectral modeling of the generation rate under AM 1.5 illumination.

The parameters $D(T,B)$ and $L(T,B)$ respectively denote the diffusion coefficient and the diffusion length in the presence of a magnetic field and temperature coupled with irradiance with $T=f(G)$.

The values of a_i and b_i, proposed by Noor S. Mohammad in the three-term ap-

proximation of the generation rate in silicon under AM 1.5 illumination, are defined as follows (Table 1).

Table 1. The coefficients a_i and b_i under AM 1.5 illumination.

$a_1 = 6.13 \times 10^{20}$	$a_2 = 0.54 \times 10^{20}$	$a_3 = 0.0991 \times 10^{20}$
$b_1 = 6630$	$b_2 = 1000$	$b_3 = 130$

2.2.2. Solution of the Continuity Equation

The solution to the continuity equation takes the following form [22]:

$$\delta_n(x,y,z) = \sum_{j=0}^{+\infty}\sum_{k=0}^{+\infty} Z_{j,k}(z)\cos(C_j x)\cos\left(\frac{C_k}{\sqrt{\theta}}y\right) \tag{5}$$

C_j and C_k are the eigenvalues of the transcendental equations, determined respectively from the boundary conditions provided:

$$D(T,B)\left.\frac{\partial\delta_n(x,y,z)}{\partial x}\right|_{x=\pm\frac{g_x}{2}} = \pm S_g\delta_n\left(x=\pm\frac{g_x}{2},y,z\right) \quad \text{and}$$

$$D(T,B)\left.\frac{\partial\delta_n(x,y,z)}{\partial y}\right|_{y=\pm\frac{g_y}{2}} = \pm S_g\delta_n\left(x,y=\pm\frac{g_y}{2},z\right) \tag{6}$$

The nonlinear relationships C_j and C_k are given by:

$$C_j\tan\left(C_j\frac{g_x}{2}\right) = \frac{S_g}{D(T,B)} \quad \text{and} \quad C_k\tan\left(\frac{C_k}{\sqrt{\theta}}\frac{g_y}{2}\right) = \frac{S_g\sqrt{\theta}}{D(T,B)} \tag{7}$$

The transcendental coefficients C_j and C_k are explicitly determined using the Newton-Raphson numerical method, based on successive approximations of their roots, according to the following iterative formula:

$$u_{n+1} = u_n - \frac{f(u_n)}{f'(u_n)} \tag{8}$$

By applying the orthogonality condition of the cosine terms, the function $Z_{j,k}(z)$ is defined as follows:

$$Z_{j,k}(z) = A_{j,k}\cosh\left(\frac{z}{L_{j,k}}\right) + B_{j,k}\sinh\left(\frac{z}{L_{j,k}}\right) + \sum_{i=1}^{3} k_i e^{-b_i z} \tag{9}$$

with

$$k_i(T,B,G) = \frac{1}{D_{j,k}(T,B)}\frac{Ga_i\cdot\left[L_{j,k}(T,B)\right]^2}{1-b_i^2\cdot\left[L_{j,k}(T,B)\right]^2} \tag{10}$$

$$L_{j,k}(T,B) = \left(C_j^2 + C_k^2 + \frac{1}{L^2(T,B)}\right)^{\frac{-1}{2}} \tag{11}$$

and

$$D_{j,k}(T,B)=\frac{D(T,B)\left(\sin\left(C_j g_x\right)+C_j g_x\right)\left(\sin\left(\frac{C_k}{\sqrt{\theta}}g_y\right)+\frac{C_k}{\sqrt{\theta}}g_y\right)}{16\left(\sin\left(C_j\frac{g_x}{2}\right)\right)\left(\sin\left(\frac{C_k}{\sqrt{\theta}}\frac{g_x}{2}\right)\right)} \tag{12}$$

The constants $A_{j,k}(T,B,G)$ and $B_{j,k}(T,B,G)$ are determined based on the boundary conditions at the junction and the rear surface:

At the junction $z=0$,

$$D(T,B)\frac{\partial\delta_n(x,y,z)}{\partial z}\bigg|_{z=0}=Sf\,\delta_n(x,y,0) \tag{13}$$

At the Back side $z=H$,

$$D(T,B)\frac{\partial\delta_n(x,y,z)}{\partial z}\bigg|_{z=H}=Sb\delta_n(x,y,z=H) \tag{14}$$

This resolution leads to:

$$A_{j,k}(T,B,G)=\sum_{i=1}^{3}k_i\frac{\frac{1}{L_{j,k}}\left(b_i-\frac{Sb}{D(T,B)}\right)\mathrm{e}^{-b_iH}-\beta_{j,k}\left(\frac{Sf}{D(T,B)}+b_i\right)}{\frac{Sf}{D(T,B)}\beta_{j,k}+\frac{\alpha_{j,k}}{L_{j,k}}} \tag{15}$$

and

$$B_{j,k}(T,B,G)=\sum_{i=1}^{3}k_i\frac{\frac{Sf}{D(T,B)}\left(b_i-\frac{Sb}{D(T,B)}\right)\mathrm{e}^{-b_iH}+\alpha_{j,k}\left(\frac{Sf}{D(T,B)}+b_i\right)}{\frac{Sf}{D(T,B)}\beta_{j,k}+\frac{\alpha_{j,k}}{L_{j,k}}} \tag{16}$$

with

$$\alpha_{j,k}(T,B)=\frac{1}{L_{j,k}}\sinh\left(\frac{H}{L_{j,k}}\right)+\frac{Sb}{D(T,B)}\cosh\left(\frac{H}{L_{j,k}}\right) \tag{17}$$

$$\beta_{j,k}(T,B)=\frac{1}{L_{j,k}}\cosh\left(\frac{H}{L_{j,k}}\right)+\frac{Sb}{D(T,B)}\sinh\left(\frac{H}{L_{j,k}}\right) \tag{18}$$

2.3. Determination of the Photocurrent and Photovoltage

The expression for the photocurrent [14] [22] is given by:

$$J_{ph}(T,B,G)=\frac{qD(T,B)}{a^2}\int_{-\frac{a}{2}}^{\frac{a}{2}}\int_{-\frac{a}{2}}^{\frac{a}{2}}\frac{\partial\delta_n(x,y,z)}{\partial z}\bigg|_{z=0}\mathrm{d}x\mathrm{d}y \tag{19}$$

After computation, the photocurrent density is defined as follows:

$$J_{ph}(T,B,G)=qD(T,B)\sum_{j=0}^{+\infty}\sum_{k=0}^{+\infty}R_{j,k}\left(\frac{B_{j,k}}{L_{j,k}}-\sum_{i=1}^{3}k_i b_i\right) \tag{20}$$

When the dynamic recombination velocity Sf at the junction becomes sufficiently

large, a simplified expression for the short-circuit photocurrent is obtained, defined as follows:

$$J_{cc}\left(T(G),B,G\right) = \frac{qD\left(T(G),B\right)}{a^2}\sum_{j=0}^{+\infty}\sum_{k=0}^{+\infty}\frac{R_{j,k}}{L_{j,k}}\sum_{i=1}^{3}k_i\left(\frac{\left(D\left(T(G),B\right)b_i - Sb\right)\mathrm{e}^{-b_i H}}{D\left(T(G),B\right)\beta_{j,k}} + \frac{\alpha_{j,k}}{\beta_{j,k}} - b_i \cdot L_{j,k}\right) \quad (21)$$

As for the expression of the photovoltage, it is determined by the Boltzmann equation [14] [22]:

$$V_{ph}\left(T,B,G\right) = V_T \ln\left(1 + \frac{N_B}{n_i^2}\int_{-\frac{a}{2}}^{\frac{a}{2}}\int_{-\frac{a}{2}}^{\frac{a}{2}}\delta_n\left(x,y,z=0\right)\mathrm{d}x\mathrm{d}y\right) \quad (22)$$

After computation, the resulting expression is given by:

$$V_{ph}\left(T,B,G\right) = V_T \ln\left(1 + \frac{a^2 N_b}{\left(ni(T)\right)^2}\sum_{j=0}^{+\infty}\sum_{k=0}^{+\infty}R_{j,k}\left(A_{j,k} + \sum_{i=1}^{3}k_i\right)\right) \quad (23)$$

with

$$R_{j,k}\left(T,B\right) = 4\sqrt{\theta}\,\frac{\sin\left(c_j\frac{a}{2}\right)\sin\left(\frac{C_k}{\sqrt{\theta}}\frac{a}{2}\right)}{a^2 c_j c_k} \quad (24)$$

The intrinsic carrier concentration, which depends on both the temperature and the electronic band structure of the material, is defined by the relation [23]:

$$n_i\left(T(G)\right) = A\cdot\left(T(G)\right)^{\frac{3}{2}}\exp\left(-\frac{E_g}{2k_b T(G)}\right) \quad (25)$$

where A is a constant given by $A = 3.87\times10^{16}\ \mathrm{cm}^{-3}\cdot\mathrm{K}^{-3/2}$, and $E_g = 1.12\times1.6\times10^{-19}\ \mathrm{J}$ denotes the energy bandgap of silicon.

2.4. Simulation Software

Python has become one of the cornerstones of contemporary scientific programming. As an interpreted, versatile, and extensible language, its streamlined syntax promotes clear, concise, and intelligible code even in the most demanding computational contexts. Its ability to adapt to the diverse requirements of research, whether in thermal simulations, magnetic field studies, or the optimization of photovoltaic devices, makes it a tool of choice for researchers, particularly in the framework of our study.

The numerical modeling of photovoltaic devices relies on a rigorous characterization of their fundamental electronic parameters. Within the scope of this simulation, these parameters are incorporated into the transport and generation equations of the photocurrent, enabling precise evaluation of the solar cell's electrical response under various climatic and environmental conditions. The corresponding values are summarized in **Table 2**.

Table 2. Fundamental electronic parameter values.

(a)						
Parameters	Sf (cm²·s⁻¹)	Sb (cm²·s⁻¹)	Sg (cm²·s⁻¹)	Xg (cm)	x (cm)	z (cm)
Values	4×10^3	4×10^3	5×10^3	3×10^{-3}	3×10^{-3}	3×10^{-3}
(b)						
H	N_b (cm⁻³)	μ_0 (cm²·V⁻¹·s⁻¹)	K (J/K)	q (C)	m	T_0 (K)
3×10^{-3}	10^{17}	1400	1.38×10^{-23}	1.602×10^{-19}	2.5	298

3. Results and Discussion

3.1. Effect of Magnetic Field and Solar Irradiance Coupled with Temperature on Minority Carrier Density

To better understand the combined effect of solar irradiance and temperature on the excess minority carrier density, two distinct simulation profiles have been established

- The first profile (Figure 2 with $T = 293$ K) illustrates the variation of carrier density as a function of irradiance, while maintaining a constant temperature. This configuration isolates the direct impact of irradiance on carrier generation.
- The second profile examines the carrier density as a function of irradiance correlated with temperature, thereby highlighting the interdependent effects of these two physical parameters. Table 3 illustrates the variation of cell temperature as a function of irradiance with NOCT = 47˚C.

Table 3. Solar cell temperature as a function of irradiance.

C (sun)	0.2	0.4	0.6	0.8	1
T (˚C)	31.75	38.5	45.25	52	58.75

- This dual representation aims to distinguish the respective and combined contributions of irradiance and temperature on the behavior of minority carriers, with the ultimate goal of optimizing the operating conditions of solar cells exposed to varying thermal and radiative environments.

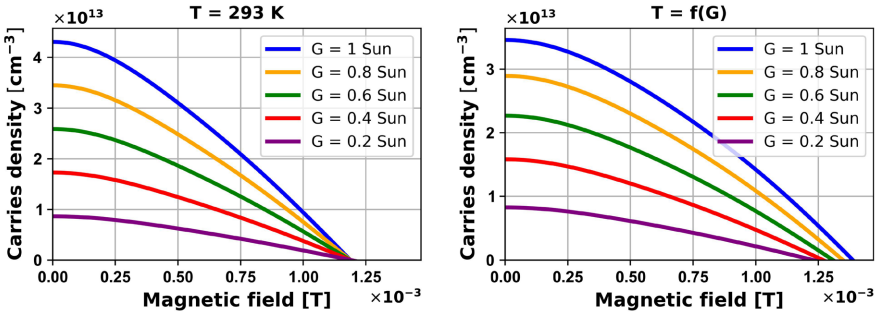

Figure 2. Carrier density profile of a polycrystalline silicon solar cell as a function of magnetic field and irradiance coupled with temperature.

The analysis of Figure 2 demonstrates that, for each irradiance level, the carrier density progressively decreases as the magnetic field intensity increases, approaching zero around 1.2 mT when temperature is held constant, and slightly beyond this threshold when temperature varies jointly with irradiance. Conversely, irradiance consistently enhances carrier density, thereby confirming the stimulating effect of incident energy on carrier generation. Nonetheless, the density remains systematically higher when temperature is not coupled with irradiance, underscoring the attenuating influence of thermal coupling on excess electron density. These findings highlight that the interaction between temperature and irradiance induces a complex dynamic, potentially constraining carrier generation under variable thermal conditions. Such behavior must be accounted for in the optimization of photovoltaic device performance within fluctuating environmental contexts.

3.2. Effect of Magnetic Field and Solar Irradiance Coupled with Temperature on Photocurrent Density

In order to deepen the understanding of the mechanisms influencing the photocurrent density in a solar cell, Figure 3 presents a series of profiles illustrating its evolution as a function of magnetic field, irradiance, and irradiance coupled with temperature.

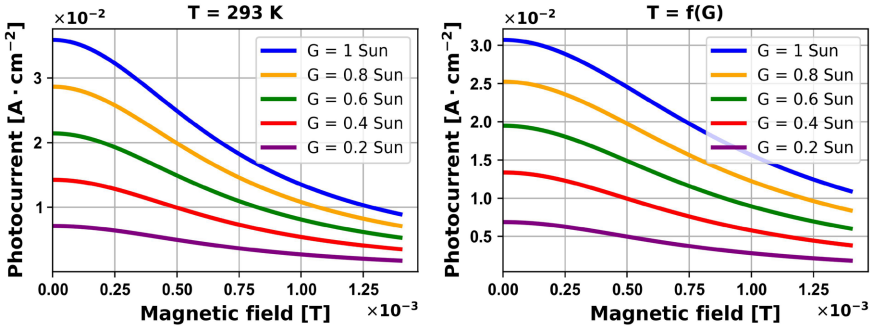

Figure 3. Photocurrent density profile of a polycrystalline silicon solar cell as a function of magnetic field under irradiance coupled with temperature.

The examination of Figure 3 highlights the evolution of the photocurrent profile as a function of magnetic field intensity, ranging from 0 to 1.4 mT. This behaviour is analysed both under constant temperature conditions (T = 293 K) and when temperature is considered as dependent on solar irradiance ($T = f(G)$), for irradiance levels varying in increments of 0.2 between 1 sun and 0.2 sun. The results reveal that an intensification of the magnetic field induces a spatial redistribution of charge carriers, thereby altering their trajectories under the effect of the Lorentz force and reducing their collection efficiency. In fact, the Lorentz force, orthogonal to both the magnetic field and the direction of carrier diffusion, causes a deflection of the electrons toward the lateral faces along the (Ox) axis. This deflection leads to a localized decrease in the photocurrent. In parallel, irradiance

enhances carrier generation and increases photocurrent density, although this effect is mitigated by the influence of the magnetic field. When temperature is coupled with irradiance, thermal recombination further reduces carrier lifetime as well as collection efficiency, resulting in a photocurrent lower than that observed under constant temperature conditions.

These findings underscore the importance of distinguishing thermal effects from those related to irradiance in the analysis of photovoltaic performance, as their interaction can generate significant energy losses that must be taken into account in the design and optimization of devices.

3.3. Effect of Magnetic Field and Solar Irradiance Coupled with Temperature on Photovoltage

The photovoltage of a photovoltaic cell is significantly influenced by temperature and solar irradiance. Figure 4 presents the photovoltage profile as a function of magnetic field for various irradiance levels, both under constant temperature and when the two climatic factors are coupled.

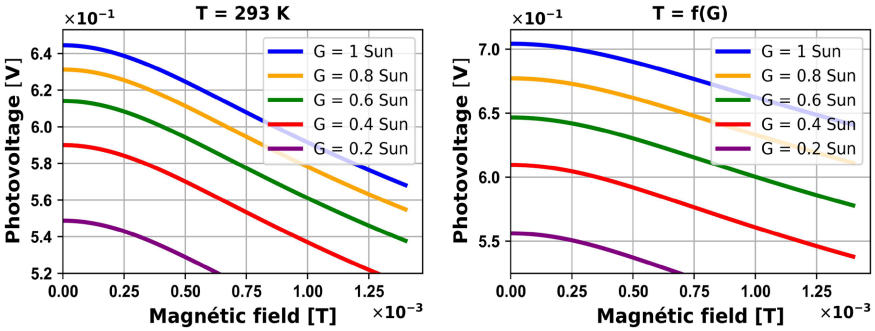

Figure 4. Photovoltage density profile of a polycrystalline silicon solar cell as a function of magnetic field under irradiance coupled with temperature.

The analysis of Figure 4 highlights the evolution of the photovoltage profile as a function of magnetic field intensity, ranging from 0 to 1.4 mT, under both constant temperature conditions (T = 293 K) and when temperature is considered as dependent on solar irradiance ($T = f(G)$), for irradiance values varying in steps of 0.2 between 1 sun and 0.2 sun. The comparative examination reveals a progressive decrease in photovoltage with increasing magnetic field intensity, consistent with the results reported by Soro *et al.* [6]. Under constant temperature, photovoltage decreases markedly as irradiance is reduced, whereas under thermal coupling ($T = f(G)$) it remains slightly higher, reflecting the dominant role of irradiance in carrier generation. This indicates that the beneficial effect of enhanced light intensity outweighs the adverse influence of temperature rise, as corroborated by previous studies [24]. In fact, solar irradiance constitutes the primary driver of photovoltaic conversion, while temperature exerts an inhibitory influence. When irradiance is sufficiently high, its beneficial effect outweighs the thermal constraints, thereby sustaining a comparatively elevated photovoltage. Finally, the decline in photovoltage

under strong magnetic fields and low irradiance is explained by the combined action of Lorentz-force deviation of carriers and reduced photon flux, which together intensify recombination and limit carrier density, thereby compromising overall efficiency.

3.4. Comparative Study with the Literature

The study underscores the decisive role of solar irradiance in the electrical performance of photovoltaic generators, particularly under the combined influence of temperature and magnetic field. Indeed, exposure to a magnetic field reduces the density of excess electrons and consequently the photocurrent, an effect further amplified by thermal and irradiance variations. These observations are consistent with the findings of Combari *et al.* [25], who demonstrated that the application of a magnetic field to silicon photovoltaic modules leads to a marked decrease in carrier density and overall efficiency. Similarly, the work of Afonso *et al.* [26] confirms the joint influence of irradiance and temperature, with the former stimulating carrier generation while the latter enhances recombination. Thus, the convergence of these results with prior studies validates the proposed model and highlights that the magnetic field, in conjunction with thermal and radiative variations, constitutes a critical factor in the assessment and optimization of photovoltaic performance.

4. Conclusion

The study highlights the decisive role of solar irradiance in the performance of photovoltaic generators, particularly under the combined influence of temperature and magnetic field. Exposure to the latter reduces the density of excess electrons and thus the photocurrent, a decrease further accentuated by thermal and radiative variations. Hence, rigorous sizing, optimized thermal management, and precise irradiance control are required to ensure the durability and efficiency of photovoltaic cells, especially in constrained environments. However, the absence of extensive experimental validation and the limited consideration of real environmental conditions (humidity, dust, solar spectrum) remain significant limitations. These limitations call for further analysis across diverse climatic contexts, the integration of *in situ* measurements, the development of multiphysics models, and the exploration of new cell architectures better adapted to thermal and magnetic constraints.

Declaration

This study did not receive any external funding. It was entirely conducted and supported by the authors.

Conflicts of Interest

The authors declare no conflicts of interest regarding the publication of this paper.

References

[1] Martial, Z., Issa, Z., Boubacar, S., Mahamadi, S., Sanna, T. and Dieudonné Joseph, B. (2017) The Effect of Magnetic Field on the Efficiency of a Silicon Solar Cell under an Intense Light Concentration. *Advances in Science and Technology Research Journal*, **11**, 133-138. https://doi.org/10.12913/22998624/69699

[2] Soro, B., Zoungrana, M., Zerbo, I., Savadogo, M. and Bathiebo, D.J. (2017) 3-D Modeling of Temperature Effect on a Polycrystalline Silicon Solar Cell under Intense Light Illumination. *Smart Grid and Renewable Energy*, **8**, 291-304. https://doi.org/10.4236/sgre.2017.89019

[3] Savadogo, M., Soro, B., Konate, R., Sourabié, I., Zoungrana, M., Zerbo, I., *et al*. (2020) Temperature Effect on Light Concentration Silicon Solar Cell's Operating Point and Conversion Efficiency. *Smart Grid and Renewable Energy*, **11**, 61-72. https://doi.org/10.4236/sgre.2020.115005

[4] Savadogo, M., Konfe, A., Sourabie, I., Soro, B., Konate, R., Zoungrana, M., *et al*. (2021) Light Concentration Solar Cell: Temperature Proper and Dynamic Effects on Electrical Parameters Determined by Using J-V and P-V Characteristics. *Global Journal of Pure and Applied Sciences*, **27**, 341-347. https://doi.org/10.4314/gjpas.v27i3.10

[5] Mahamadi, S., Pegdwindé, O.F.O., Adama, O., Lamine, Z., Martial, Z. and Issa, Z. (2022) Uncooled PV Cell under Variable Light Concentration: Determination of Profiles of the Temperature, the Intrinsic Properties and the Carrier Density. *International Journal of Physical Sciences*, **17**, 96-107. https://doi.org/10.5897/ijps2022.5010

[6] Soro, B., Ouedraogo, A., Savadogo, M., Konate, R., Tchouadep, G., Zoungrana, M., *et al*. (2023) Investigation of the Behavior of a Photovoltaic Cell under Concentration as a Function of the Temperature of the Base and a Variable External Magnetic Field in 3D Approximation. *Smart Grid and Renewable Energy*, **14**, 209-220. https://doi.org/10.4236/sgre.2023.1412013

[7] Zouma, B., Maiga, A., Dieng, M., Zougmore, F. and Sissoko, G. (2009) 3D Approach of Spectral Response for a Bifacial Silicon Solar Cell under a Constant Magnetic Field. *Global Journal of Pure and Applied Sciences*, **15**, 117-124. https://doi.org/10.4314/gjpas.v15i1.44908

[8] Zoungrana, M., Zerbo, I., Savadogo, M., Tiedrebeogo, S., Soro, B. and Bathiebo, D.J. (2017) Effect of Light Intensity on the Performance of Silicon Solar Cell. *Global Journal of Pure and Applied Sciences*, **23**, 123-129. https://doi.org/10.4314/gjpas.v23i1.12

[9] Zoungrana, M., Zerbo, I., Ouedraogo, F., Zouma, B. and Zougmoré, F. (2012) 3D Modelling of Magnetic Field and Light Concentration Effects on a Bifacial Silicon Solar Cell Illuminated by Its Rear Side. *IOP Conference Series*: *Materials Science and Engineering*, **29**, Article ID: 012020. https://doi.org/10.1088/1757-899x/29/1/012020

[10] Ahmadpanah, F.S., Orouji, A.A. and Gharibshahian, I. (2021) Improving the Efficiency of CIGS Solar Cells Using an Optimized P-Type Cztsse Electron Reflector Layer. *Journal of Materials Science*: *Materials in Electronics*, **32**, 22535-22547. https://doi.org/10.1007/s10854-021-06740-6

[11] Amiri, M., Eskandarian, A. and Ziabari, A.A. (2020) Performance Enhancement of Ultrathin Graded Cu(InGa)Se2 Solar Cells through Modification of the Basic Structure and Adding Antireflective Layers. *Journal of Photonics for Energy*, **10**, Article ID: 024504. https://doi.org/10.1117/1.jpe.10.024504

[12] Diasso, A., Sam, R., Yacouba Traoré, N. and Zougmoré, F. (2020) Effects of External Magnetic Field and Air Mass on Space Charge Region Width Extension of a Bifacial Solar Cell Front Side Illumination. *International Journal of Energy and Power Engineering*, **9**, Article 29. https://doi.org/10.11648/j.ijepe.20200903.11

[13] Ouedraogo, M., Traore, N.Y., Diasso, A., Sam, R. and Zougmore, F. (2025) Effect of Magnetic Field and Temperature on the Excess Minority Carrier Density in the Base of a Radial Junction Solar Cell. *Nano Select*, **6**, e70054. https://doi.org/10.1002/nano.70054

[14] Dieng, A., Zerbo, I., Wade, M., Maiga, A.S. and Sissoko, G. (2011) Three-Dimensional Study of a Polycrystalline Silicon Solar Cell: The Influence of the Applied Magnetic Field on the Electrical Parameters. *Semiconductor Science and Technology*, **26**, Article ID: 095023. https://doi.org/10.1088/0268-1242/26/9/095023

[15] Zoungrana, M., Zebro, I., Sere, A., Zouma, B. and Zougmore, F. (2009) 3D Study of Bifacial Silicon Solar Cell under Intense Light Concentration and under External Constant Magnetic Field. *Global Journal of Engineering Research*, **10**, 113-124.

[16] Kabré, A., Bonkoungou, D. and Koalaga, Z. (2024) Analysis of the Effect of Temperature and Relative Humidity on the Reliability of a Photovoltaic Module. *Advances in Materials Physics and Chemistry*, **14**, 165-177. https://doi.org/10.4236/ampc.2024.148013

[17] Laronde, R., Charki, A. and Bigaud, D. (2010) Reliability of Photovoltaic Modules Based on Climatic Measurement Data. *International Journal of Metrology and Quality Engineering*, **1**, 45-49. https://doi.org/10.1051/ijmqe/2010012

[18] Sahu, N.C., Nanda, A.B., Bhol, S., Jena, A.K. and Rout, P. (2020) Reliability Assessment and Cost Estimation of a Hybrid Renewable Micro-Grid System. In: Sharma, R., Mishra, M., Nayak, J., Naik, B. and Pelusi, D., Eds., *Lecture Notes in Networks and Systems*, Springer, 169-182. https://doi.org/10.1007/978-981-15-8218-9_14

[19] Furlan, J. and Amon, S. (1985) Approximation of the Carrier Generation Rate in Illuminated Silicon. *Solid-State Electronics*, **28**, 1241-1243. https://doi.org/10.1016/0038-1101(85)90048-6

[20] Diop, M.S., Ba, H.Y., Thiam, N., Diatta, I., Traore, Y., Ba, M.L., *et al*. (2019) Surface Recombination Concept as Applied to Determinate Silicon Solar Cell Base Optimum Thickness with Doping Level Effect. *World Journal of Condensed Matter Physics*, **09**, 102-111. https://doi.org/10.4236/wjcmp.2019.94008

[21] Pelanchon, F., Sudre, C. and Moreau, Y. (1992) Solar Cells under Intense Light Concentration: Numerical and Analytical Approaches. 11*th European Photovoltaic Solar Energy Conference*, Montreux, 12-16 October 1992, 12-16.

[22] Dugas, J. (1994) 3D Modelling of a Reverse Cell Made with Improved Multicrystalline Silicon Wafers. *Solar Energy Materials and Solar Cells*, **32**, 71-88. https://doi.org/10.1016/0927-0248(94)90257-7

[23] Diatta, I., Ly, I., Wade, M., Diouf, M.S., Mbodji, S. and Sissoko, G. (2016) Temperature Effect on Capacitance of a Silicon Solar Cell under Constant White Biased Light. *World Journal of Condensed Matter Physics*, **6**, 261-268. https://doi.org/10.4236/wjcmp.2016.63024

[24] Sun, C., Zou, Y., Qin, C., Zhang, B. and Wu, X. (2022) Temperature Effect of Photovoltaic Cells: A Review. *Advanced Composites and Hybrid Materials*, **5**, 2675-2699. https://doi.org/10.1007/s42114-022-00533-z

[25] Combari, D.U., Ramde, E.W., Korgo, B., Saré, R., Zoungrana, M. and Zerbo, I. (2021) Investigating the Effect of Inclination Angle of Magnetic Field Vector on Silicon PV Modules. *International Journal of Photoenergy*, **2021**, 1-6. https://doi.org/10.1155/2021/8818869

[26] Afonso, D., Mesbahi, O., Bouich, A. and Tlemçani, M. (2025) Influence of Long-Term and Short-Term Solar Radiation and Temperature Exposure on the Material Properties and Performance of Photovoltaic Panels: A Comprehensive Review. *Energies*, **18**, Article 5072. https://doi.org/10.3390/en18195072